The Effect of Pressure on the Plume Divergence in the Hall Thruster

Avi Cohen-Zur, Amnon Fruchtman, *Senior Member, IEEE*, and Alon Gany

***Abstract*—The plume divergence in the Hall thruster due to the plasma pressure is analyzed by deriving and solving envelope equations. The evolution of the electron temperature and the radial expansion of the plasma beam are calculated self-consistently. The rate of decrease of the electron temperature due to the plasma radial expansion is affected by heat conduction along the plasma propagation. For the annular plasma jet exiting the Hall thruster, approximated as a slab, it is found that if the coefficient of the heat conductivity is large, the cooling of the electrons of the expanding plasma beam is small, and consequently, the plume divergence is larger. For the plasma beam approximated as cylindrical beyond the point at which it crosses the thruster axis, we show that a large amount of heat conduction does not slow the electron cooling. The plume divergence due to the plasma pressure is therefore smaller. The electron temperature is also affected by the intensity of the magnetic field beyond the cathode. A radial magnetic field at the thruster exhaust inhibits a large cross-field heat flux. On one hand, the smaller heat conductivity of the magnetized plasma results in a cooling of the electrons as they cross the magnetic field. On the other hand, however, the reduced mobility of the magnetized electrons results in an ambipolar electric field that tends to heat the electrons. We show that there is an optimal intensity of the magnetic field, at which the temperature of the electrons that cross the magnetic field is minimal and at which, therefore, the plume divergence is minimal.**

***Index Terms*—Hall effect, Hall thruster, heat conductivity, plasma thrusters, plume divergence.**

I. Introduction

A CRUCIAL issue in the Hall thruster performance is achieving a better plume collimation. Decreasing the plume divergence should reduce the erosion of surfaces, particularly the solar panels, by impacting ions. Furthermore, a less divergent plume should result in a smaller interference with the radio frequency transmission that is used for communication. Two major sources for the plume divergence are the curvature of the magnetic field lines and the radial force exerted on the plasma by the electron pressure. A considerable theoretical and experimental effort has been made over the past few years in order to understand the evolution of the plume [1]–[30]. Encouraging indications for a reduction of plume divergence have been found when the magnetic field configuration [28] or the electrodes [5] were manipulated. We have recently analyzed the role of the magnetic field curvature in increasing the plume divergence and made suggestions as to what magnetic field profile can minimize that divergence [27]. In this paper, we analyze the effect of the plasma (electron) pressure on the plume divergence, which, outside the acceleration region, seems to be the main reason for the plume divergence.

The plume divergence analyzed here is caused by the transverse electric fields that are induced by the magnetic field curvature and by the electron pressure. These transverse electric fields affect the fast ions during their axial motion and, to a larger extent, the slower ions that are generated through charge-exchange collisions with slow neutral atoms. We do not include ion collisions in the analysis here. In the desirable case of high propellant utilization, the slower component of the ion population generated through charge exchange is small and does not significantly affect the plasma flow or the electrostatic fields. However, even a small number of these resulting slow ions can cause severe damage to the satellite. But if their number is small, the forces exerted on the slow ions, their trajectories, and the estimated damage can be determined, to lowest order, from the plasma flow and electric fields as calculated in the present model. If the slow population is larger, one should resort to a more detailed numerical calculation [7], [9], [15], [18], [29].

As common in Hall thruster modeling [3], [4], [9], [10], [12]–[15], [18], [19], [29], we employ a fluid model for the electrons in the plume. In our model, we assume the usual form for the transport coefficients including the form for the heat conductivity also assumed in recent numerical calculations [12], [29]. It is important to note, as we show here for a typical Hall thruster, that the mean free path of the electrons is quite large in certain regions in the plume, and therefore, the applicability of these fluid models is limited. A collisionless model for the electrons may enable further understanding of the plume behavior. The results of the fluid models are nevertheless valid for the higher power denser beams in Hall thrusters and for other dense plasma beams in laboratory and space.

The plume divergence in the Hall thruster due to the plasma pressure is analyzed here by deriving and solving a set of envelope equations. The evolution of the electron temperature and the radial expansion of the plasma beam are calculated self-consistently. Although our envelope equations cannot provide

Manuscript received November 3, 2007; revised April 11, 2008. First published October 21, 2008; current version published November 14, 2008. This research was supported in part by the United States–Israel Binational Science Foundation, Jerusalem, Israel, under Grant 9800145, and in part by the Hellen Asher Foundation for Space Research.

A. Cohen-Zur was with the Department of Sciences, H.I.T.—Holon Institute of Technology, Holon 58102, Israel, and with the Faculty of Aerospace Engineering, Technion—Israel Institute of Technology, Haifa 32000, Israel. He is now with WALES, Ltd., Ramat Gan 52522, Israel (e-mail: aerbnac@aerodyne.technion.ac.il).

A. Fruchtman is with the Department of Sciences, H.I.T.—Holon Institute of Technology, Holon 58102, Israel (e-mail: fnfrucht@hit.ac.il).

A. Gany is with Faculty of Aerospace Engineering and Asher Space Research Institute, Technion—Israel Institute of Technology, Haifa 32000, Israel (e-mail: gany@techunix.technion.ac.il; gany@tx.technion.ac.il).

Color versions of one or more of the figures in this paper are available online at http://ieeexplore.ieee.org.

Digital Object Identifier 10.1109/TPS.2008.2004224

as detailed a picture of the plume as some of the numerical simulations do, they have the advantage, due to their simplicity, of allowing a calculation of the plasma flow up to a large distance. This is done by requiring the plasma flow to satisfy appropriate boundary conditions at infinity. In addition, we derive analytical expressions for the flow at asymptotic limits that provide us with a useful insight into the physical processes that govern the plume divergence.

Since the source of the plume divergence is the plasma pressure, the extent of the divergence depends on the evolution of the electron temperature. If both magnetic field and heat conductivity are zero, the electron temperature decreases adiabatically to zero as the plasma expands and the asymptotic value of the plasma perpendicular velocity can be determined analytically. The rate of decrease of the electron temperature due to the plasma radial expansion is affected by heat conduction along the plasma propagation. For the annular plasma jet exiting the Hall thruster, approximated as a slab, it is found that if the coefficient of the heat conductivity is large, the cooling of the electrons of the expanding plasma beam is small, and consequently, the plume divergence is larger. For the plasma beam, approximated as cylindrical beyond the point at which it crosses the thruster axis, we show that a large amount of heat conduction does not slow the electron cooling. The plume divergence due to the plasma pressure is therefore smaller.

Detailed recent measurements [22] of the evolution of the electron temperature in the Hall thruster have shown that the rate of decrease can be associated with an effective polytropic exponent that falls between the isothermal and adiabatic values. It has been concluded that the electron heat conduction plays a major role in the evolution of the electron temperature [22]. The model developed here could be used for analyzing this role of the heat conductivity.

The electron temperature is also affected by the magnitude of the magnetic field beyond the cathode. A radial magnetic field at the plasma exhaust inhibits a large cross-field heat flux. On one hand, the smaller heat conductivity of the magnetized plasma results in a cooling of the electrons as they cross the magnetic field. On the other hand, however, the reduced mobility of the magnetized electrons results in an ambipolar electric field that tends to heat the electrons. We show that there is an optimal intensity of the magnetic field, at which the temperature of the electrons that cross the magnetic field is minimal and at which, therefore, the plume divergence is minimal.

In Section II, we present the 2-D equations, and in Section III, we derive the envelope equations. These equations allow us to address the inherently 2-D problem by simply solving a set of ordinary differential equations. In Section IV, we reanalyze the isothermal case [1], [6] that provides us with an upper bound on the plume divergence for a given initial electron temperature. In Section V, we numerically solve the evolution of a slab plasma beam with finite heat conductivity. The aforementioned two opposite effects of the magnetic field are shown and discussed, following an earlier version of this analysis [16].

In Sections VI and VII, the very different effects of heat conduction on the plume divergence for the two geometries are described. In Section VI, the effect of the heat conductivity on the divergence of a slab beam is analyzed. We present in more detail a previous analysis [20] that included analytical expressions for the plume divergence for an asymptotically large coefficient of the heat conductivity. It is shown that the large amount of conducted heat by a slab beam is converted downstream into electron thermal energy and, consequently, into a large radial velocity and a large divergence of the plasma beam.

Beyond the point at which it crosses the thruster axis, we approximate the plasma beam as cylindrical. We show in Section VII that the heat conducted by a cylindrical beam is decoupled from the electron thermal energy convected by the plasma beam. The plume divergence in the cylindrical case is therefore smaller.

II. Two-Dimensional Equations

We describe here a quasi-neutral azimuthally symmetric plasma beam propagating in the z-direction across a magnetic field. The magnetic field is approximated as having an r component only, which is perpendicular to the direction of the beam, and the axial z component is neglected. We later discuss the consequences of this approximation. The plasma current has an azimuthal component only. This is because our calculation applies to the region beyond the cathode surface, a surface approximately transverse to the z-direction at which the net axial current vanishes. Beyond the cathode surface, at the plume side, the electric axial current is neutralized, and the ion and electron axial velocities are equal. The position of that cathode surface, at which the current becomes zero, has to be found through a fully 2-D numerical calculation. As we show, some of our results strongly depend on the assumed location of the cathode surface.

We therefore model the plasma beam by writing fluid equations for the identical ion and electron density n and radial and axial velocities v_r and v_z. Since in the Hall thruster the ion temperature is much smaller than the electron temperature T_e, we take the ion temperature in the model as zero. We also assume that the ions are unmagnetized. The plasma dynamics is therefore governed by the continuity equation

$$\frac{1}{r}\frac{\partial}{\partial r}(\mathrm{rnv}_r)+\frac{\partial}{\partial z}(\mathrm{nv}_z)=0 \tag{1}$$

the two components of the momentum equation

$$\begin{aligned}\frac{1}{r}\frac{\partial}{\partial r}\left(rm_i n v_r^2\right)+\frac{\partial}{\partial z}(m_i n v_z v_r) &= -\frac{\partial}{\partial r}(nT_e)\\ \frac{1}{r}\frac{\partial}{\partial r}(rm_i n v_r v_z)+\frac{\partial}{\partial z}\left(m_i n v_z^2\right) &= -\frac{\partial}{\partial z}(nT_e)-m_e n v_z\frac{\omega_c^2}{\nu}\end{aligned} \tag{2}$$

and the energy equation

$$\begin{aligned}&\frac{1}{r}\frac{\partial}{\partial r}\left\{\left[\frac{m_i}{2}\left(v_r^2+v_z^2\right)+\frac{5}{2}T_e\right]rnv_r\right\}\\ &+\frac{\partial}{\partial z}\left\{\left[\frac{m_i}{2}\left(v_r^2+v_z^2\right)+\frac{5}{2}T_e\right]nv_z\right\}=-\frac{1}{r}\frac{\partial(rq_r)}{\partial r}-\frac{\partial q_z}{\partial z}\end{aligned} \tag{3}$$

where m_i and m_e are the ion and electron masses, ν and $\omega_c = eB/m_e$ are the electron collision and cyclotron frequencies, and $q_{z,r}$ is the heat flux in the (z,r)-direction. Furthermore, e and B are the elementary charge and the intensity of the radial magnetic field. The first term on the right-hand side (RHS) of the first equation in (2) is the electron pressure gradient, which equals the electric force exerted radially outward on the ions. The second term on the RHS of the second equation in (2) expresses the axial magnetic force due to the azimuthal electron current and the radial magnetic field. Within a fluid model, similar to the one that we employ here, the effect of heat flux on the plume evolution was considered in [12] and [29] and on the plasma dynamics in the acceleration channel in [31].

For completion, we also derive in a standard way the equation for the entropy. Employing (1)–(3), we write the heat balance equation for the electrons $nT_e\vec{\nabla}\cdot\vec{v} + \vec{\nabla}\cdot(3/2)nT_e\vec{v} + \vec{\nabla}\cdot\vec{q} = m_e n v_z^2\omega_c^2/\nu$, in which the last term on the RHS is the rate of heating. Using the identity $\vec{\nabla}\cdot(nT_e\vec{v}) = n\vec{v}\cdot\vec{\nabla}T_e$, we then derive the equation $T_e\vec{\nabla}\cdot sn\vec{v} + \vec{\nabla}\cdot\vec{q} = m_e n v_z^2\omega_c^2/\nu$ for the entropy per particle $s \equiv \ln(T_e^{3/2}/n)$. In cylindrical coordinates, this equation becomes

$$T_e\left[\frac{1}{r}\frac{\partial(rsnv_r)}{\partial r} + \frac{\partial(snv_z)}{\partial z}\right] = -\frac{1}{r}\frac{\partial(rq_r)}{\partial r} - \frac{\partial q_z}{\partial z} + m_e n v_z^2\frac{\omega_c^2}{\nu}. \quad (4)$$

This equation shows clearly that the entropy flux is constant in the absence of heating and heat conduction.

In Section III, we derive a set of envelope equations.

III. Envelope Equations

We address two specific cases, both of interest to the Hall thruster. One case is of a thin annular beam that is approximated as a planar slab in which r_0 is the inner radius of the annulus. The second case is of a solid cylindrical beam in which $r_0 = 0$ denotes the axis of symmetry. We derive envelope equations that are suitable for the two cases, either a thin annular beam [16], [20] or a solid cylindrical beam. We integrate the above equations multiplied by $2\pi r$ with respect to r between $r = r_0$ and $r = r_1$, where r_1 denotes the outer edge of the beam. The plasma beam, as it exits the thruster channel, can be approximated by the slab beam of the first case, while after it expands radially and crosses the thruster cylindrical axis, it can be described by the cylindrical beam of the second case. In both cases, as a result of the radial integration over the entire plume, we obtain quasi-1-D equations for the radially averaged plasma variables at each axial location.

Since there is no net radial flux, all first terms on the left-hand side (LHS) of (1)–(3) vanish upon the radial integration. So does the first term on the RHS of (3). The integrated equations are the continuity equation

$$\Gamma(z) \equiv \int_{r_0}^{r_1} 2\pi r n v_z\, dr = \Gamma_0 = \text{const.} \quad (5)$$

the r component of the momentum equation

$$\frac{d}{dz}T_r = F_r \quad (6)$$

where

$$T_r(z) \equiv \int_{r_s}^{r_1} 2\pi r m_i n v_z v_r\, dr$$

$$F_r(z) \equiv -\int_{rs}^{r_1} 2\pi r\frac{\partial}{\partial r}(nT_e)\, dr \quad (7)$$

the z component of the momentum equation

$$\frac{dT_z}{dz} = F_z \quad (8)$$

where

$$T_z(z) \equiv \int_{r_0}^{r_1} 2\pi r\left(nm_i v_z^2 + nT_e\right) dr$$

$$F_z(z) \equiv -\int_{r_0}^{r_1} 2\pi r\left(m_e n v_z\frac{\omega_c^2}{\nu}\right) dr \quad (9)$$

and the energy equation

$$\Gamma_\varepsilon(z) \equiv \int_{r_0}^{r_1} 2\pi r\left\{\left[\frac{m_i}{2}\left(v_r^2 + v_z^2\right) + \frac{5}{2}T_e\right] n v_z + q_z\right\} dr$$
$$= \Gamma_{\varepsilon 0}$$
$$= \text{const.} \quad (10)$$

Here, $r_s = (r_0 + r_1)/2$ for the slab and $r_s = r_0$ for the solid cylinder. The assumption of a radial magnetic field only holds for the thin annular beam. The cylindrical beam will be assumed unmagnetized.

We now transform the equations for fluid variables that depend on z and r to equations for the radially averaged quantities that depend on z only, where the averaged quantity $\langle f\rangle(z)$ is defined as

$$\langle f\rangle(z) \equiv \frac{\int_{r_s}^{r_1} 2\pi r n(z,r) f(z,r) dr}{\int_{r_s}^{r_1} 2\pi r n(z,r) dr}. \quad (11)$$

The temperature T_e is approximated as constant across the plume $T_e(z,r) \cong T_e(z)$ due to the plasma high heat conductivity along magnetic field lines. So are $\omega_c(z,r) \cong \omega_c(z)$ and $\nu(z,r) \cong \nu(z)$. Moreover, we also approximate the axial velocity v_z as constant across the plume $v_z(z,r) \cong v_z(z)$ since v_z is approximately constant at the thruster exit plane. We therefore write

$$\Gamma_0 \equiv v_z(z)\int_{r_0}^{r_1} 2\pi r n\, dr. \quad (12)$$

With this last relation, we can express the integrals above as

$$T_r(z) \equiv m_i \frac{\Gamma_0}{2} \langle v_r \rangle \quad F_r(z) \equiv -T_e(z) \frac{\Gamma_0}{2 v_z(z)} \left\langle \frac{\partial \ln n}{\partial r} \right\rangle \tag{13}$$

$$T_z(z) \equiv \frac{\Gamma_0}{v_z} \left(m_i v_z^2 + T_e \right) \quad F_z(z) \equiv -\Gamma_0 m_e \frac{\omega_c^2}{\nu}. \tag{14}$$

We express the averaged quantities in the following form:

$$\left\langle \frac{\partial \ln n}{\partial r} \right\rangle = -\frac{\alpha}{a} \tag{15}$$

where $a \equiv r_1 - r_s$. The energy equation becomes

$$\Gamma_{\varepsilon 0} = \Gamma_0 \left[\frac{m_i}{2} \left(\langle v_r^2 \rangle + v_z^2 \right) + \frac{5}{2} T_e \right] + \frac{\Gamma_0}{v_z} \left\langle \frac{q_z}{n} \right\rangle.$$

For completeness, we also present the quasi-1-D equation for the entropy

$$T_e \frac{d}{dz} \langle s \rangle = -\frac{d}{dz} \left(\frac{1}{v_z} \left\langle \frac{q_z}{n} \right\rangle \right) + m_e v_z \frac{\omega_c^2}{\nu}. \tag{16}$$

We now use an explicit expression for q_z

$$q_z = -\kappa \frac{dT_e}{dz} \tag{17}$$

in which the coefficient for heat conductivity is κ and the approximate $\langle 1/n \rangle = 1/n$ where $n = n(z)$ is the radially averaged plasma density at z. The governing equations for $\langle v_r \rangle$, v_z, and T_e become

$$m_i \frac{d}{dz} \langle v_r \rangle = \alpha \frac{T_e(z)}{v_z(z) a(z)} \tag{18}$$

$$\frac{d}{dz} \left(m_i v_z + \frac{T_e}{v_z} \right) = -m_e \frac{\omega_c^2}{\nu} \tag{19}$$

$$\frac{dT_e}{dz} = \frac{n v_z}{\kappa} \left[\frac{m_i}{2} \left(\alpha_2 \langle v_r \rangle^2 + v_z^2 \right) + \frac{5}{2} T_e - \frac{\Gamma_{\varepsilon 0}}{\Gamma_0} \right]. \tag{20}$$

Again, we express the averaged quantity as

$$\langle v_r^2 \rangle = \alpha_2 \langle v_r \rangle^2. \tag{21}$$

We need an additional equation for the beam thickness a, the "averaged streamline" equation, of the form

$$\frac{da}{dz} = \alpha_1 \frac{\langle v_r \rangle}{v_z} \tag{22}$$

where α_1 is the assumed constant ratio between the transverse velocity at the plume boundary and the average transverse velocity.

To proceed, we write an explicit expression for κ

$$\kappa = 3.16 \frac{n T_e}{m_e \nu} \left(\frac{1}{\omega_c^2 / \nu^2 + 1} \right). \tag{23}$$

From the last equation, it follows that in the region of finite magnetic field in which $\omega_c \gg \nu$, the resulting heat coefficient is very small. As the magnetic field vanishes, κ becomes larger.

We now write the equations (18)–(20) and (22) in a dimensionless form

$$\frac{da}{d\xi} = \alpha_1 \frac{u}{v} \tag{24}$$

$$\frac{du}{d\xi} = \alpha \frac{c^2}{v a} \tag{25}$$

$$\frac{d}{d\xi} \left(v + \frac{c^2}{v} \right) = -f_B \tag{26}$$

$$\frac{dc^2}{d\xi} = \frac{1}{\kappa_n} \left(\alpha_2 u^2 + v^2 + 5c^2 - \Gamma_{\varepsilon n} \right) \tag{27}$$

for the dimensionless unknowns u, v, and c^2 with the dimensionless independent variable ξ

$$u \equiv \frac{\langle v_r \rangle}{v_0} \quad v \equiv \frac{v_z}{v_0} \quad c^2 \equiv \frac{T_e}{m_i v_0^2} \quad \xi \equiv \frac{z}{a_0}. \tag{28}$$

In the following equations, f_B is the normalized magnetic force, κ_n is the normalized heat conductivity, and $\Gamma_{\varepsilon n}$ is the ratio of the total energy flux to the directed kinetic ion flux:

$$f_B = \frac{m_e}{m_i} \frac{a_0 \nu_d}{v_0}, \qquad \nu_d \equiv \frac{\omega_c^2}{\nu}$$

$$\kappa_n = 2 \times 3.16 \times \frac{S}{\Gamma_0 a_0} \frac{n T_e}{\nu m_e} \left(\frac{1}{\omega_c^2 / \nu^2 + 1} \right)$$

$$\Gamma_{\varepsilon n} = \frac{2 \Gamma_{\varepsilon 0}}{\dot{m} v_0^2}. \tag{29}$$

Here, ν and ω_c are the electron collision and cyclotron frequencies, and $\dot{m} \equiv m_i \Gamma_0$ is the mass flow rate, $v_0 = \sqrt{2 e \phi_A / m_i}$, with ϕ_A being the applied voltage, and $a_0 = a(0)$. In the normalized equations and in the rest of this paper, a is normalized to a_0. Although there is no self-similar solution for the 2-D equations, we assume here that the averaging parameters α, α_1, and α_2 remain constant along the plume axis. Additionally, $S = S(z)$ is the effective cross section of the beam, which is defined as follows:

$$S = \pi (4 r_s)^{2-d} a^d \tag{30}$$

where $d = 1$ for a slab geometry, $d = 2$ for a cylindrical geometry. We note that if ν is proportional to n, the dimensionless κ_n varies with the beam cross section and with the temperature. We also define the normalized conducted heat as

$$\Delta \equiv \frac{2\kappa}{m_i v_0^2 n v_z} \frac{dT_e}{dz} = \Gamma_{\varepsilon n} - \left(\alpha_2 u^2 + v^2 + 5c^2 \right).$$

The electron collision frequency is the sum of electron-ion collision frequency ν_{e-i} and of additional "anomalous" collisions frequency ν_{ano}. We assume that the plasma is nearly fully ionized so that electron-neutral collisions are negligible. We therefore write

$$\nu = \nu_{e-i} \left(1 + \frac{\nu_{\text{ano}}}{\nu_{e-i}} \right), \quad \nu_{e-i} = 2.91 \times 10^{-6} \ln \Lambda \, n \, T_e^{-3/2} \tag{31}$$

where $\ln \Lambda$ is the Coulomb logarithm, n is in units per cubic centimeter, and T_e is in electronvolts. The anomalous collision frequency was taken as the Bohm diffusion $\nu_{\rm ano} = \alpha_B \omega_c$, with a somewhat smaller than the classical value of the Bohm coefficient, i.e., $\alpha_B = 1/80$ (as in [32] and [33]). With this expression, we write the normalized heat conductivity in the form

$$\kappa_n = \kappa_{nac} \frac{c^{2p} a^d}{(\omega_c^2/\nu^2 + 1)\,(1 + \nu_{\rm ano}/\nu_{e-i})}. \tag{32}$$

For the heat conductivity, we take

$$\kappa_{nac} = 3.48 \times 10^{-7} \left(\frac{m_i}{m_e}\right) \frac{a_0 T_{e0}^p \pi}{\dot{m} \ln \Lambda\, c_0^{2p}} \times \left(\frac{4r_0}{a_0}\right)^{2-d} \left(\frac{\rm kg}{\rm m/s(eV)^p}\right), \quad p = \frac{5}{2}. \tag{33}$$

We solve the equations by specifying boundary conditions upstream, i.e.,

$$v(0) = 1 \quad a(0) = 1 \quad u(0) = u_0 \quad c^2(0) = c_0^2 \tag{34}$$

and we require that

$$c^2(\infty) = 0 \tag{35}$$

which determines the value of $\Gamma_{\varepsilon n}$ and the amount of heat conducted Δ.

In Section IV, we present a brief analysis of the isothermal case using our set of equations. The results of that analysis are similar to previous analyses of the isothermal case that provided self-similar solutions of the flow [1], [6].

IV. Isothermal Case

In the isothermal case, $c^2(z) = c_0^2$ is constant. We also assume that the magnetic field is zero so that the axial velocity is constant as well, i.e., $v(z) = 1$. We combine (24) and (25). The resulting equation

$$\frac{d^2 a}{d\xi^2} = \frac{\beta^2}{2a}, \quad \beta^2 \equiv 2\alpha\alpha_1 c_0^2 \tag{36}$$

is integrated to

$$a'^2 = a'(0)^2 + \beta^2 \ln a, \quad a' \equiv \frac{da}{d\xi}; \quad a'(0) = \alpha_1 u_0 \tag{37}$$

and further to

$$\operatorname{erf}\left[i\sqrt{\frac{a'(0)^2}{\beta^2} + \ln a}\right] - \operatorname{erf}\left[i\frac{a'(0)}{\beta}\right] = \frac{i\beta}{\sqrt{\pi}} \xi \exp\left[\frac{a'(0)^2}{\beta^2}\right]. \tag{38}$$

The two last relations are combined for the following relation between a' and ξ:

$$\operatorname{erf}\left(\frac{ia'}{\beta}\right) - \operatorname{erf}\left(\frac{ia'(0)}{\beta}\right) = \frac{i\beta}{\sqrt{\pi}} \xi \exp\left[\frac{a'(0)^2}{\beta^2}\right]. \tag{39}$$

This last relation provides us with the value of ξ for which a' becomes of order unity. Since β is usually much smaller than unity, for $a'/\beta \gg 1$ we approximate $\operatorname{erf}(ia'/\beta) \approx i\beta/(a'\sqrt{\pi}) \exp(a'^2/\beta^2)$ so that

$$\xi \cong \frac{1}{a'} \exp\left[\frac{a'^2 - a'(0)^2}{\beta^2}\right] + \frac{i\sqrt{\pi}}{\beta} \operatorname{erf}\left(\frac{ia'(0)}{\beta}\right) \exp\left[-\frac{a'(0)^2}{\beta^2}\right]. \tag{40}$$

The first term on the RHS shows a strong dependence on the electron temperature. If the temperature is higher by a factor of two, the location where the plume reaches a certain value of a' is shortened by a factor $\exp(a'^2/2\beta^2)$.

Since the plume expansion is so sensitive to the value of the electron temperature, it is important to examine the case that the temperature may vary. The processes that affect the temperature evolution are transfer of energy between convected thermal energy and directed energy, heat conduction, and plasma heating by the electric field. In Section V, we present a numerical solution without the assumption of isothermal electrons.

V. Numerical Solution of the Equations in a Slab Geometry

Equations (24)–(27) were solved for various values of the input parameters, using the method described in the Appendix. Note that while in the isothermal case the structure of the equations is the same for both geometries, when heat conductivity is taken into account, the solution depends on the geometry. We start with the slab geometry, which is a good approximation as long as $a \ll r_0$ for the thin annular plasma beam exiting the thruster. Equation (33) holds with $d = 1$.

We denote the axial location of the cathode surface as $z = 0$ so that the plume propagates in the region $z > 0$. The profile of the magnetic field intensity was taken as

$$B = B_{\rm peak} \exp\left[-\frac{(z - z_m)^2}{L_m^2}\right] \tag{41}$$

with $z_m < 0$ being the axial location inside the thruster channel where the intensity of the magnetic field is maximal and L_m being the characteristic width. Figs. 1–3 present the results of the calculation for a typical case $B_{\rm peak} = 200$ G and $L_m = 20$ mm. The thruster dimensions are the channel half width $a_0 = 10$ mm and a median radius of $r_s = 40$ mm. The propellant in all the examples in this paper is assumed to be xenon. At the cathode, the temperature is taken as $T_e = 3$ eV, the transverse velocity as $u_0 = 0$, and $\phi_A = 300$ V. The particle flux Γ_0 was calculated for $\dot{m} = 5.32$ mg/s. The mass flow rate and the initial beam energy assumed the above values in all the numerical calculations in this paper. The values of the three averaging parameters α, α_1, and α_2 were taken here as unity.

The axial profiles are presented in the near field only, even though the calculation domain spans temperatures approaching zero. The solid and dashed lines show the results as found by the two different numerical schemes in the two different regions, as described in the Appendix. The location of the cathode

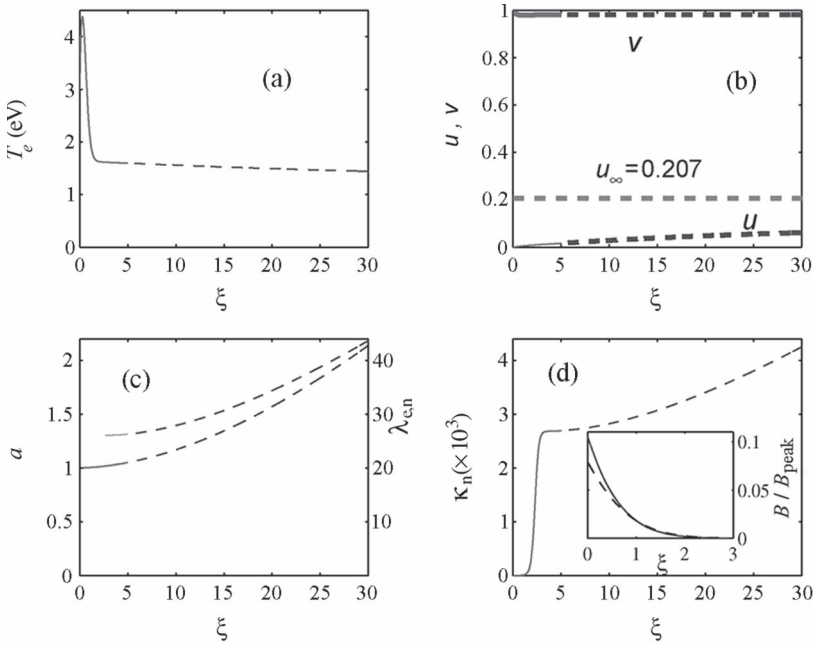

Fig. 1. Characteristic slab plume profiles for the parameters mentioned in the text: (a) T_e which increases in the magnetized region, (b) the radial and axial velocities, denoted is the asymptotic radial velocity, (c) the width of the beam and the electron mean-free-path, and (d) the heat conductivity, much smaller in the magnetized region. The dashed line corresponds to the computational domain in which the magnetic field was taken as zero. In the inset are shown the normalized radial component (solid line) and axial component (dashed line) of the magnetic field at $r = a_0/2$.

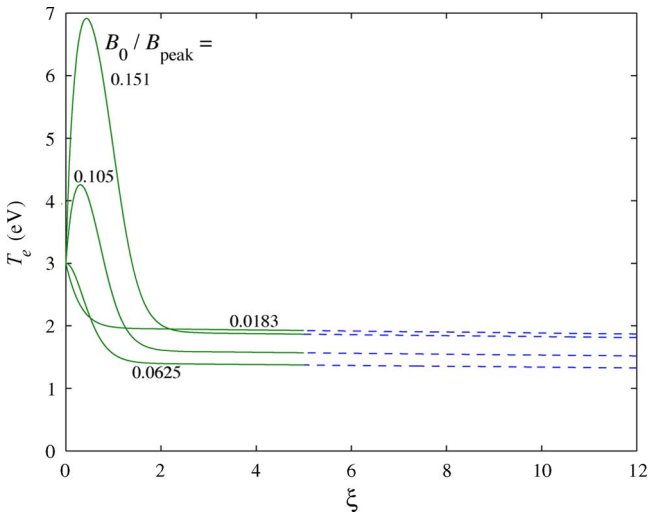

Fig. 2. Profiles of the electron temperature for different values of z_m in (41), denoted is the value of $B_0/B_{\rm peak}$. The parameters, except for z_m, are as in Fig. 1. The different profiles correspond to different axial locations of the cathode surface. The curve for which $B_0/B_{\rm peak} = 0.21$ is as in Fig. 1.

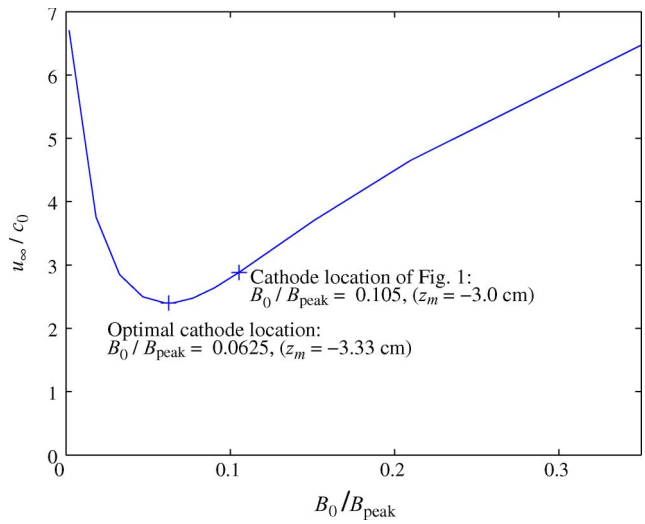

Fig. 3. Asymptotic radial velocity as a function of B_0 or, equivalently, as a function of the axial location of the cathode surface in the magnetized region. The parameters, except for z_m, are as in Fig. 1.

surface is specified in Fig. 1 by choosing $z_m = -30$ mm. An important result that follows this assumed location of the cathode is the temperature behavior within the magnetic field region [Fig. 1(a)]. The temperature increases sharply as the magnetically impeded electrons are forced to cross the magnetic field at the same velocity as do the ions. The increase in temperature is due to the work of the ambipolar electric field, hence, the ion kinetic energy (and velocity in the z-direction) decreases [Fig. 1(b)]. The ambipolar electric field points in the direction toward the thruster exit, opposite the direction of the electric field inside the thruster. This reversal of the electric field direction and the associated nonmonotonic profile of the electric potential were pointed out for the first time in [3]. We generalize the analysis in [3], in which electrons were assumed isothermal, by solving the electron heat balance equation for the evolution of the electron temperature. As the magnetic field intensity drops, κ is increased, allowing heat to flow downstream [Fig. 1(d)]. The temperature gradient in that region is inversely proportional to the fast-varying coefficient of heat conductivity as the total heat flux varies more slowly (the total energy flux is constant). As a result, in that region, the temperature gradient is very large, and it becomes much smaller in the unmagnetized region. As the magnetic field vanishes, the values of the plasma parameters match the values of the zero

magnetic field calculations (dashed line). Since only the near field is presented ($z/a_0 \leq 30$), the asymptotic approach of T_e to 0 and of u to $u_\infty = u(z = \infty)$ is not apparent in Fig. 1.

As seen in Fig. 1, the magnetic field has two opposing effects on the electron temperature and further on the plume divergence. On one hand, the magnetic field inhibits heat flux, and therefore, the temperature drop is enhanced in the magnetized region, resulting in a reduced plume divergence. On the other hand, the magnetic field induces an ambipolar electric field that heats the electrons, resulting in an increased plume divergence. Due to the competition between the two processes that govern the evolution of the temperature, the reduction of heat conductivity, and the introduction of the ambipolar electric field, the dependence of the plume divergence on the magnetic field intensity turns out to be nonmonotonic. An optimal intensity of the magnetic field exists, at which the electron temperature of the plume exiting the magnetized region is lowest and the final plume divergence minimal. The dependencies of the electron temperature and the plume divergence on the intensity of the magnetic field are exhibited in Figs. 2 and 3. Fig. 2 shows the profiles of the electron temperature for various different values of z_m, reflecting how deep into the magnetic field the cathode surface is located. For the assumed identical $B_{\rm peak}$, L_m, and $T_e(0)$, there is an optimal value of z_m or, equivalently, magnetic field intensity at the cathode. The asymptotic radial velocity of the plasma beam is shown in Fig. 3 as a function of the intensity of the magnetic field at the cathode, i.e., $B_0 = B(z = 0)$. In the figures, the dependence on z_m is shown by denoting $B_0/B_{\rm peak} = \exp(-z_m^2/L_m^2)$. The existence of an optimal configuration is also apparent there.

Our calculation demonstrates in detail that the propagation of a zero-current plasma beam across a magnetic field should be accompanied by an axially nonmonotonic profile of the electric potential, as has been also shown previously in [3], and probably also by an axially nonmonotonic profile of the electron temperature. We are aware of only one measurement in which the electron temperature was found to increase along the plume propagation [2]. The monotonically decreasing electron temperature usually found could have resulted, according to the present analysis, from higher-than-expected electron heat conductivity. A more plausible explanation is that, usually, the cathode surface is located beyond the magnetized region, resulting in the measured monotonically decreasing electron temperature. Indeed, for the magnetic field of the SPT-100 as shown in [10, Fig. 3(a)], the cathode is found to be tied to field lines that cross the plume about two channel widths downstream, corresponding to $z_m \cong -50$ mm. The single measurement in which the electron temperature was found not to decrease monotonically [2] resulted probably from a configuration in which the cathode surface was located inside the magnetic field. It would be interesting to explore experimentally how changing the position of the cathode could affect the axial location of the cathode surface and the plume divergence.

We emphasize that it is not easy to deduce the axial location of the cathode surface across the plasma beam from the known position of the cathode itself. In fact, it is not clear whether such a cathode surface actually exists. The current distribution could be 2-D so that the axial current decreases gradually over a certain spatial extent—from its maximal value, which is the discharge current, to zero.

We note that for a magnetic field of intensity on the order of 100 G and electrons of a temperature of several electronvolts, the Larmor radius is on the order of 1 mm, which is significantly smaller than a characteristic scale length. The mean free path of the electrons in the unmagnetized region, however, is much larger. Fig. 1(c) shows the normalized mean free path of the electron in the unmagnetized region, i.e., $\lambda_{e,n} \equiv v_t/(\nu_{e-i}a_0)$, where the electron thermal velocity is $v_t \equiv \sqrt{8T_e/\pi m_e}$. The plume radius doubles its size along about one mean free path. The validity of these commonly used fluid models is marginal for the SPT-100 for these values of the parameters.

The inset in Fig. 1(d) shows the normalized radial and axial components of the magnetic field at $r = a_0/2$. The normalized radial component of the magnetic field is $B/B_{\rm peak}$, where B is given by (41). The normalized axial component of the magnetic field is then $B_z/B_{\rm peak} = -2[r(z - z_m)/L_m^2]\exp[-(z - z_m)^2/L_m^2]$, resulting in $|B_z|/B = 2[r(z - z_m)/L_m^2]$. It is seen in the figure that in the bulk of the plume, at $r = a_0/2$, the two components of the magnetic field are comparable. Because the axial component of the magnetic field has a radially confining effect on the plasma, by neglecting the axial component in our model, we actually overestimate the plume divergence near the exit from the thruster. However, as seen in Fig. 1, the divergence due to the plasma pressure in the magnetized region is small, and the main effect there is the possible heating of the electrons.

In Section VI, we further examine the effect of the heat conductivity on the evolution of the plume beyond the magnetized area.

VI. Effect of Heat Conductivity in a Slab Beam

Here, we analyze the effect of heat conductivity on the evolution of the plume when there is no magnetic field. We therefore assume that the magnetic field is zero for $z \geq 0$. Because the magnetic field is zero, i.e., $f_B = 0$ in (26), the plasma momentum in the axial direction is constant. By also employing (35), we obtain

$$v + \frac{c^2}{v} = 1 + c_0^2, \qquad v_\infty = 1 + c_0^2. \tag{42}$$

We first address the slab geometry, i.e., $d = 1$ in (32) and (33), but we keep p unspecified. We have

$$\kappa_n = \kappa_{nac} c^{2p} a. \tag{43}$$

In the slab geometry, the equations are reduced to one differential equation, which is given by

$$\frac{du}{dc^2} = \frac{\alpha \kappa_{nac} c^{2(1+p)}}{v\left(\alpha_2 u^2 + v^2 + 5c^2 - \Gamma_{\varepsilon n}\right)} \tag{44}$$

in which v is specified by (42) and $\Gamma_{\varepsilon n}$ is determined by the requirement that

$$\Delta(\infty) = \Gamma_{\varepsilon n} - v_\infty^2 - \alpha_2 u_\infty^2 = 0, \qquad \text{when } d = 1. \tag{45}$$

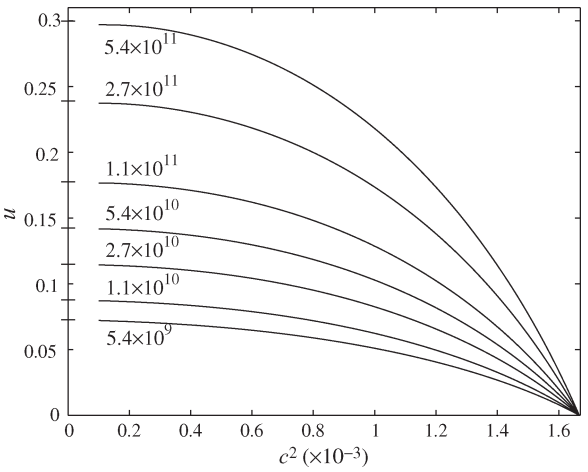

Fig. 4. Unmagnetized slab beam: the radial velocity u as a function of c^2 for different values of κ_{nac}. For each such value u_∞ is denoted on the vertical axis. The initial value of c^2, 0.00167, corresponds to $T_e = 1$ eV when the applied voltage is 300 V.

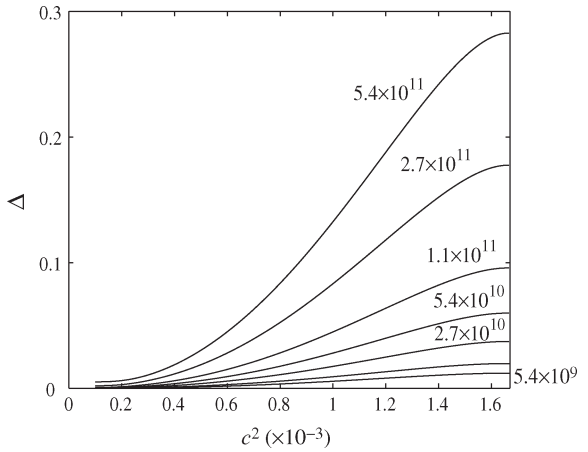

Fig. 5. Unmagnetized slab beam: the conducted heat as a function of c^2 for various values of κ_{nac}.

The equation relates u and c^2 and is decoupled from the equations for the dependence on ξ. The last requirement determines the value of the eigenvalue $\Gamma_{\varepsilon n}$. It is important to note that in the slab geometry, the conducted heat at infinity is zero. All the heat at the cathode, i.e., $\Delta(0) = \Gamma_{\varepsilon n} - 1 - 5c_0^2$, is converted into convected thermal energy and then into directed kinetic energy. In the slab geometry, therefore, the directed kinetic energy and the plume expansion are potentially large if the heat conductivity is large.

Fig. 4 shows u versus T_e, while Fig. 5 shows the conducted heat versus T_e, both for various values of κ_{nac}. In Figs. 4–6, the values of the three averaging parameters α, α_1, and α_2 were taken as 3/2, 4, and 16/5, respectively. It is seen in the figures that the heat conducted ends up in the kinetic energy associated with the radial velocity of the ions. In both figures, $\phi_A = 300$ V, and $p = 5/2$. The applied voltage, the ion (xenon) mass, and the initial temperature determine the value of c_0^2, while the value of κ_{nac} is arbitrarily specified in order to examine the effect of the heat conductivity. The radial velocity is larger when κ_{nac} is larger.

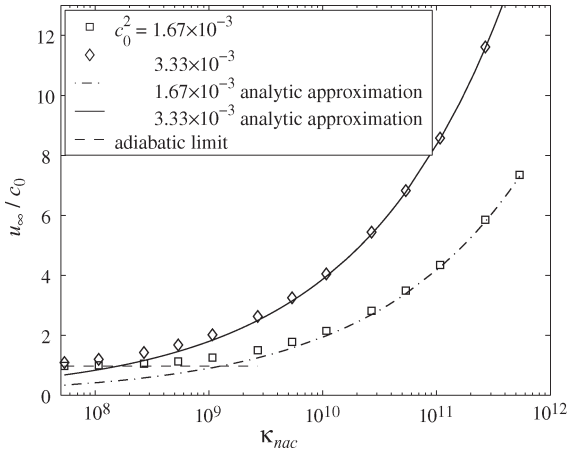

Fig. 6. Unmagnetized slab beam: the asymptotic radial velocity as a function of κ_{nac} for two initial electron temperatures. A comparison of the analytical and numerical results. Shown is also the adiabatic case.

We can actually derive analytical expressions for the asymptotic limit of large values of κ_{nac} [20]. At that limit, we approximate

$$v \cong 1 \quad \alpha_2 u^2 + v^2 + 5c^2 - \Gamma_{\varepsilon n} \cong \alpha_2 u^2 + 1 - \Gamma_{\varepsilon n},$$
$$\alpha_2 u_\infty^2 + 1 - \Gamma_{\varepsilon n} = 0. \quad (46)$$

In this approximation, the convected electron thermal energy is much smaller than the conducted heat. Equation (44) is then simplified to

$$\frac{du}{dc^2} = \frac{\alpha \kappa_{nac} c^{2(1+p)}}{\alpha_2 \left(u^2 - u_\infty^2\right)}. \quad (47)$$

This simplified equation is integrated to

$$\left(\frac{u^3 - u_0^3}{3}\right) - u_\infty^2 (u - u_0) = \frac{\alpha \kappa_{nac}}{\alpha_2} \left[\frac{c^{2(2+p)} - c_0^{2(2+p)}}{2+p}\right] \quad (48)$$

where we allowed an initial finite radial velocity $u(z=0) = u_0$. The expression for u_∞ when $u_0 = 0$ is [20]

$$u_\infty = \left[\frac{3\alpha \kappa_{nac} c_0^{2(2+p)}}{2\alpha_2 (2+p)}\right]^{1/3}$$
$$p = \frac{5}{2} \Longrightarrow u_\infty$$
$$= \left(\frac{\alpha \kappa_{nac}}{3\alpha_2}\right)^{1/3} c_0^3. \quad (49)$$

Thus, the solution in the slab geometry is characterized by all the conducted heat being transformed into thermal energy and into perpendicular kinetic energy. The perpendicular velocity is unbounded in that geometry and increases with the initial velocity and with the size of the coefficient of heat conduction. Fig. 6 shows the dependence of u_∞ on κ_{nac} for two values of initial electron temperature. The agreement with the analytical expressions [see (49) for $p = 5/2$] is excellent.

The growth of the radial velocity of the plasma beam as predicted by the analysis of this section is too small to explain the plume divergence observed in the near field of the thruster. For the measured electron temperatures, the plane at which the plume crosses the axis of symmetry of the thruster should be farther away than it actually is. We thus conclude that the main cause of the plume divergence near the exit of the plasma thruster is not the plasma pressure, but probably the magnetic field curvature.

We turn to examine the plume divergence beyond the crossover plane. We approximate the plasma beam there as cylindrical.

VII. Effect of Heat Conductivity in a Cylindrical Beam

The governing equations in the case of a cylindrical beam are (24)–(27), which, for $d = 2$ and with no magnetic field, become

$$\frac{dc^2}{d\xi} = \frac{1}{\kappa_{nac} c^{2p} a^2} \left(\alpha_2 u^2 + v^2 + 5c^2 - \Gamma_{\varepsilon n}\right). \tag{50}$$

Because the area in the cylindrical beam is proportional to the square of the radius, an equation relating u and c^2 decoupled from ξ cannot be derived as was done for the slab case. The Appendix describes the numerical scheme for solving the equations in the cylindrical case. These equations describe the basic, and of a general nature, phenomenon of a radial expansion of a beam (plasma or neutral gas) of a cylindrical geometry.

In the cylindrical geometry, there is weak coupling only between the conducted heat and the convected electron thermal energy. As the coefficient of heat conductivity or the initial electron temperature is increased, the heat conducted is large. At the limit of large conducted heat, that heat flux is constant along the beam. Let us examine this asymptotic case. The last equation is approximated as

$$\begin{aligned} \frac{dc^2}{d\xi} &= -\frac{\beta_c}{\kappa_{nac} c^{2p} a^2} \\ \beta_c &\equiv -\left(\alpha_2 u^2 + v^2 + 5c^2 - \Gamma_{\varepsilon n}\right) \\ &\cong \text{const.} > 0. \end{aligned}$$

Combining this equation with (24) in which we approximate $v \cong 1$, we write the following equation:

$$k\frac{d^2k}{dt^2} = -A_c t^{1/(1+p)}, \qquad k \equiv \frac{1}{a}; \quad t \equiv \left(\frac{c}{c_0}\right)^{2p+2}; \qquad A_c \equiv \alpha\alpha_1 \left[\frac{c_0^{2p+3}\kappa_{nac}}{\beta_c(p+1)}\right]^2 \tag{51}$$

to be solved for

$$k(1) = 1 \quad \frac{dk}{dt}(1) = 0 \quad k(0) = 0 \quad A_c = A_c(p) \text{ eigenvalue.} \tag{52}$$

Note that the numerical value that A_c assumes turns out to be independent of κ_{nac}. For example, for $p = 5/2$, A_c is found numerically to be $\simeq 1.85$. From here, the value of the conducted heat is determined and found to be

$$\beta_c = \sqrt{\frac{\alpha\alpha_1}{A_c}} \frac{c_0^{2p+3}\kappa_{nac}}{(p+1)} \tag{53}$$

which shows a strong dependence on the initial temperature. The velocity is found to be

$$u = \sqrt{\frac{\alpha}{\alpha_1 A_c}} c_0 \frac{dk}{dt}. \tag{54}$$

The velocity (54) is proportional to the acoustic velocity and is not larger for a larger coefficient of the heat conductivity κ_{nac}. The temperature profile $t(k)$ is independent of the heat conductivity as well at this limit.

The lack of coupling between the conducted heat and the convected thermal energy in the cylindrical beam is a major result of this paper. A beam of a cylindrical cross section can conduct heat at a high rate, while this conducted heat does not affect much the plume divergence.

For the Hall thruster, the plasma beam can be approximated as a cylindrical beam beyond the crossover of the thruster axis. At that plane, the beam (regrettably ...) already has a high radial velocity. It is useful to derive linear solutions for the equations in this limit of large conducted heat. In fact, we derive analytical solutions for the case of a cylindrical beam with a large flux of conducted heat.

We approximate the radial velocity to lowest order as constant by

$$u_0 = \sqrt{\frac{\alpha}{\alpha_1 A_c}} c_0 \frac{dk}{dt} \tag{55}$$

and as before

$$k(1) = 1 \quad k(0) = 0 \qquad A_c = A_c(p) \text{ eigenvalue.} \tag{56}$$

we find that

$$t u_0 = k\sqrt{\frac{\alpha}{\alpha_1 A_c}} c_0 \tag{57}$$

which, with (56), yields

$$A_c = \frac{\alpha}{\alpha_1}\left(\frac{c_0}{u_0}\right)^2 \quad \beta_c = \frac{\alpha_1 u_0 c_0^{2p+2}\kappa_{nac}}{(p+1)}. \tag{58}$$

The linear solutions are therefore

$$\begin{aligned} c^2 &= c_0^2 a_l^{-\frac{1}{p+1}} \\ u &= u_0 + u_1(\infty)\left(1 - a_l^{-\frac{1}{p+1}}\right) \\ a &= a_l + \alpha_1 u_1(\infty)\left[\xi - \left(\frac{p}{p+1}\right)\left(a_l^{\frac{p}{p+1}} - 1\right)\right] \end{aligned} \tag{59}$$

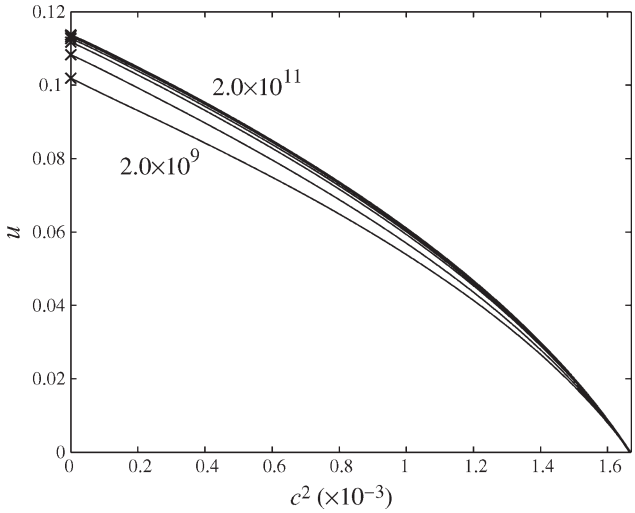

Fig. 7. Unmagnetized cylindrical beam: the radial velocity as a function of the electron temperature for various values of κ_{nac}.

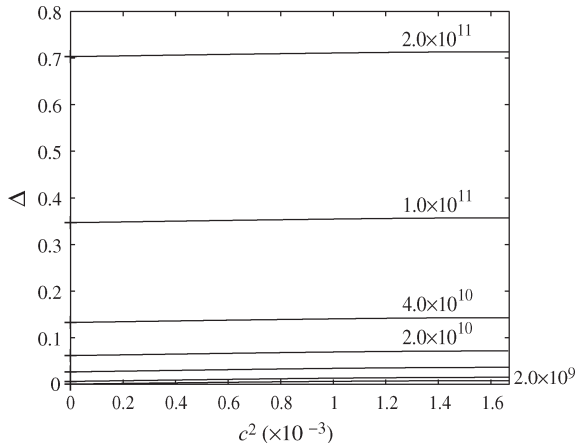

Fig. 8. Unmagnetized cylindrical beam: the conducted heat as a function of the electron temperature for various values of κ_{nac}.

where $a_l = 1 + \alpha_1 u_0 \xi$ and the asymptotic value of the velocity is

$$u_1(\infty) = \frac{\alpha c_0^2 (p+1)}{\alpha_1 u_0}. \tag{60}$$

The conditions for the heat conductivity to be considered large and for the linearization to be justified are

$$\beta_c = \frac{\alpha_1 u_0 c_0^{2p+2} \kappa_{nac}}{v(p+1)} \gg 1 \qquad \frac{\alpha c_0^2 (p+1)}{\alpha_1 u_0^2} \ll 1. \tag{61}$$

We now present numerical results for the cylindrical case, in which $p = 5/2$. Fig. 7 shows u as a function of c^2 for various values of κ_{nac}. It is seen in the figure that as κ_{nac} grows, the velocity reaches asymptotically a limit value. Similarly in Fig. 8, the normalized conducted heat is shown to be larger when κ_{nac} is larger, but it does not change along the beam propagation. It is apparent in the figure that the conducted heat and the convected thermal energy are decoupled. The asymptotic

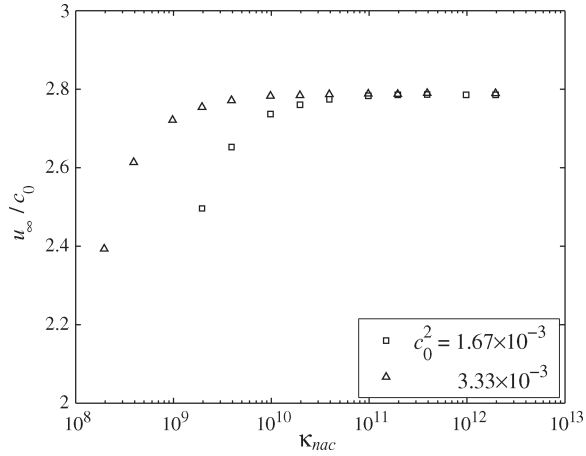

Fig. 9. Unmagnetized cylindrical beam: the asymptotic radial velocity as a function of κ_{nac} for two initial electron temperatures. Apparent is the asymptotic limit.

limit of u_∞ as the conductivity coefficient is increased is also apparent in Fig. 9. The asymptotic limits of u_∞/c_0 for a large κ_{nac} for two different values of c_0^2 are seen to be the same. In Figs. 7–9, the values of the three averaging parameters α, α_1, and α_2 were taken as 8/3, 15/8, and 75/64, respectively. A comparison between the analytical linear solution and the numerical solution is presented both in Figs. 10 and 11 for $u_0 = 0.5$ and $\alpha = \alpha_1 = \alpha_2 = 1$. In Fig. 11 these results are presented for small values of ξ. The validity of the fluid model for the Hall thruster beyond the crossover plane is examined in Fig. 11. The mean free path is calculated for $a_0 = 8$ cm. As the plume cross section grows, the plasma density decreases, and the electron mean free path grows. For the parameter values in this example, at a distance of several tens of centimeters from the crossover plane, a kinetic or a particle picture would be more appropriate for modeling the electron dynamics.

VIII. Summary

We have presented an analysis of the plume divergence due to the electron pressure of a plasma beam for both a slab and a cylindrical geometry. We have shown that the effect of the heat conductivity is very different in the two different geometries. We have unfolded the two opposite effects of the transverse magnetic field across which the plasma beam propagates. If the number of charge-exchange collisions is not large, then their effect could also be incorporated into an extended version of the present model.

As common in Hall thruster modeling, we employed here a fluid model for the electrons in the plume. We showed that because of the relatively large mean free path of the electron in the plume, the validity of such fluid models is marginal. Nevertheless, it could be, as it often happens in plasmas, that various fluctuations introduce a higher effective collision frequency that makes the fluid picture valid. In addition, the present model could be applied to other denser plasma beams (including higher power Hall thrusters) in which the mean free path of the electrons is smaller so that the validity of our fluid approach is clearer. At the collisionless limit, a kinetic model or particle simulations for the electrons might be needed.

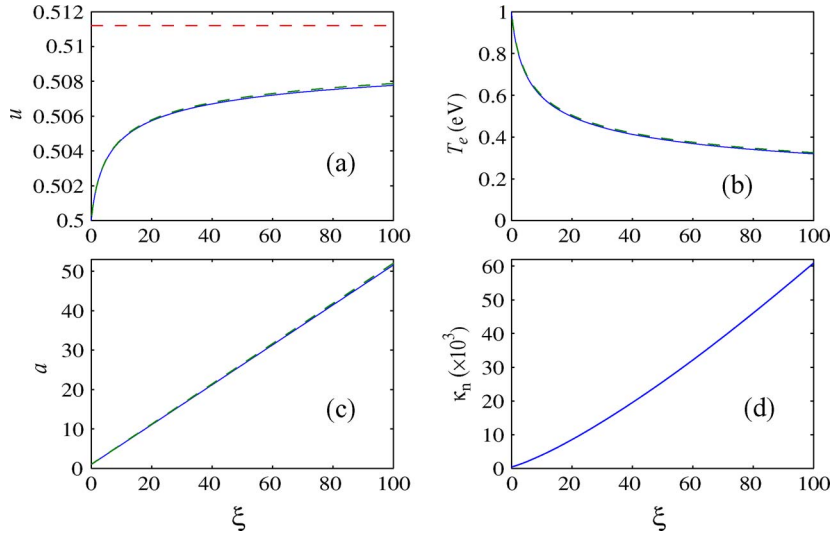

Fig. 10. Cylindrical plume profiles in the linear regime - analytical (dashed) and numerical (solid). Here, $T_{e0} = 1$ eV, $u_0 = 0.5$. The upper dashed horizontal line in (a) denotes the asymptotic limit of u.

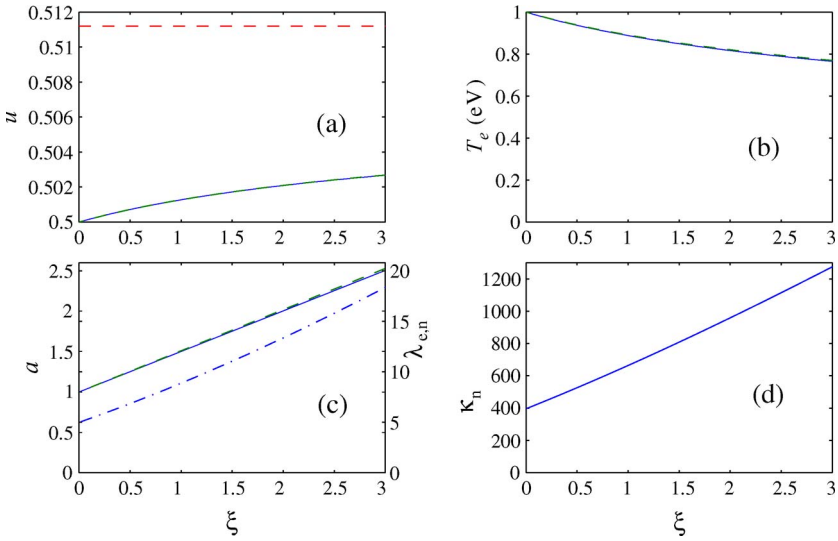

Fig. 11. Cylindrical plume profiles in the linear regime - analytical (dashed) and numerical (solid) near the crossover plane. Here, as in Fig. 10, $T_{e0} = 1$ eV, $u_0 = 0.5$. The dashed-dotted line in (c) denotes the local mean free path of the electrons if $a_0 = 8$ cm.

Our main motivation was to examine the contribution of the electron pressure to the plume divergence in the Hall thruster. We found that the measured plume divergence in the Hall thruster seems to be much larger than the plume divergence due to the electron pressure as calculated according to the model here. We therefore suggest that the electron pressure is a source of only a small part of the plume divergence, and that the magnetic field curvature, as described in our previous paper [27], is the main cause of the plume divergence. Nevertheless, the analysis here allows the calculation of the plume divergence that is expected in the Hall thruster once the plume divergence due to magnetic field curvature and other sources of divergence is minimized. Moreover, the results obtained in this paper are of a general nature and may apply to other plasma beams in laboratory and in space. The analysis here with the various asymptotic limits could provide insight into such other plasma beams that are dominated by radial forces due to electron pressure.

APPENDIX

As mentioned in Section V, in the case of no magnetic field in a slab geometry, the equation for v becomes an algebraic relation, and the equations for u and c^2 are independent of ξ and are decoupled from the equation for a. This allows us to set the temperature as the independent variable and solve for u without dealing with infinite values of ξ and a. Employing (45), we write (44) in which $p = 5/2$ as

$$\frac{du}{dc^2} = \frac{\alpha \kappa_{nac} c^7}{v\left(\alpha_2 u^2 + v^2 + 5c^2 - v_\infty^2 - \alpha_2 u_\infty^2\right)}. \tag{62}$$

As mentioned in Section VI, we seek a solution in which $u \longrightarrow u_\infty$ and the denominator vanishes as $c^2 \to 0$. In order to find the regular solution near $c^2 = 0$, we expand the unknowns u, v, and $\Delta = \alpha_2 u^2 + v^2 + 5c^2 - v_\infty^2 - \alpha_2 u_\infty^2$ in powers of c

near $c=0$, using (62) and the relation $v+c^2/v=v_\infty$. For the slab geometry, the expansions become

$$\begin{aligned} u &= u_\infty + u_2c^2 + u_4c^4 + u_6c^6 + u_7c^7 \\ u_2 &= -\frac{3}{2\alpha_2 u_\infty} \\ u_4 &= \frac{1}{2u_\infty}\left(\frac{1}{\alpha_2 v_\infty^2} - u_2^2\right) \\ u_6 &= \frac{1}{u_\infty}\left(\frac{1}{\alpha_2 v_\infty^4} - u_2u_4\right) \\ u_7 &= -\frac{\alpha\kappa_{nac}}{3v_\infty} \\ v &= v_\infty - \frac{c^2}{v_\infty} - \frac{c^4}{v_\infty^3} - \frac{2c^6}{v_\infty^5} - \frac{5c^8}{v_\infty^7} \\ \Delta &= -\frac{2\alpha\alpha_2\kappa_{nac}u_\infty}{3v_\infty}c^7, \quad u_\infty \text{ parameter.} \end{aligned} \tag{63}$$

The values of u_∞ and v_∞ are determined by specifying the values of u and v at a certain value of c^2 upstream. The axial velocity v is found from its algebraic relation [similar to (42)], which, for the case of a finite magnetic field, assumes the form

$$v^2 + \frac{c^2}{v} = v_{B0}^2 + \frac{c_{B0}^2}{v_{B0}}. \tag{64}$$

In this expression, the subscript $B0$ denotes a downstream location where the beam can be regarded as unmagnetized. We use the power expansion to approximate u for a small c^2 and integrate (62) in the upstream direction.

When the transverse magnetic field is present, the equations are dependent on ξ through the variation of the magnetic field intensity, and the entire set of equations (24)–(27) must be solved numerically. A shooting method is used to match the solutions in the two regimes. First, a downstream integration of the set of equations is performed down to a point where the magnetic field is negligible. This determines the values of v_{B0} and c_{B0}^2 required for the next stage. Then, an upstream integration of the decoupled equation $[u(c^2)]$ is performed from the vicinity of $c^2=0$ (found by the power series expansion) to the corresponding value of c_{B0}^2 (at the downstream end of the magnetized regime). The parameter u_∞ is adjusted by the search algorithm of the shooting method until the value of u is matched from both sides of the regime interface. This scheme also results in finding the corresponding value for the constant energy flux $\Gamma_{\varepsilon n}=v_\infty^2+\alpha_2u_\infty^2$, which can be viewed as the eigenvalue of the problem. Once the value for $\Gamma_{\varepsilon n}$ is found, the other flow variables (a and ξ) in the zero magnetic field regime are solved as downstream as desired.

In the case of cylindrical geometry, the equation for $u(c^2)$ is not decoupled from a, and we defined $k\equiv 1/a=k(c^2)$. In this case, the power expansions yield

$$\begin{aligned} k &= -\alpha_1\frac{2}{7}\frac{\kappa_{nac}u_\infty}{\Delta_\infty v_\infty}c^7 \\ u &= u_\infty - \frac{7}{2}\frac{\alpha}{\alpha_1 u_\infty}c^2, \quad u_\infty,\ \Delta_\infty \quad \text{parameters.} \end{aligned} \tag{65}$$

The solution was found for the zero magnetic field regime only, therefore, (42) is used for finding v_∞. The shooting method performs a search over both parameters—the heat flux (Δ_∞) and the lateral velocity (u_∞) simultaneously—yielding the initial conditions $u(c^2=c_0^2)=u_0$, and $k(c^2=c_0^2)=1$.

ACKNOWLEDGMENT

The authors would like to thank Prof. N. J. Fisch, Dr. Y. Raitses, Dr. J. Ashkenazy, Prof. A. Gallimore, and G. Makrinich for the helpful discussions.

REFERENCES

[1] D. E. Parks and I. Katz, "A preliminary model of ion beam neutralization," presented at the 14th Int. Electric Propulsion Conf., Princeton, NJ, 1979, Paper AIAA 79-2049.

[2] J. M. Fife, "Hybrid-PIC Modeling and Electrostatic Probe Survey of Hall Thrusters," Ph.D. dissertation, Dept. Aeronautics Astronautics, MIT, Cambridge, MA, Sep. 1998.

[3] M. Keidar and I. D. Boyd, "Effect of a magnetic field on the plasma plume from Hall thrusters," *J. Appl. Phys.*, vol. 86, no. 9, pp. 4786–4791, Nov. 1999.

[4] D. Y. Oh, D. E. Hastings, C. M. Marrese, J. M. Haas, and A. D. Gallimore, "Modeling of stationary plasma thruster-100 thruster plumes and implications for satellite design," *J. Propuls. Power*, vol. 15, no. 2, pp. 345–357, Mar./Apr. 1999.

[5] Y. Raitses, L. A. Dorf, A. A. Litvak, and N. J. Fisch, "Plume reduction in segmented electrode Hall thruster," *J. Appl. Phys.*, vol. 88, no. 3, pp. 1263–1270, Aug. 2000.

[6] J. Ashkenazy and A. Fruchtman, "Plasma plume far field analysis," presented at the 27th Int. Electric Propulsion Conf., Pasadena, CA, 2001, Paper IEPC 01-260.

[7] I. Katz, G. Jongeward, V. Davis, M. Mandell, I. Mikellides, R. Dressler, I. Boyd, K. Kannenberg, J. Pollard, and D. King, "A Hall effect thruster plume model including large-angle elastic scattering," presented at the 37th Joint Propulsion Conf., Salt Lake City, UT, 2001, AIAA Paper 2001-3355.

[8] F. Darnon, "The SPT-100 plasma plume and its interaction with a spacecraft, from modeling to ground and flight characterization," presented at the 32nd Joint Propulsion Conf., Lake Buena Vista, FL, 1996, AIAA Paper No. 96-3196.

[9] I. G. Mikellides, G. A. Jongeward, I. Katz, and D. H. Manzella, "Plume modeling of stationary plasma thrusters and interactions with the express—A spacecraft," *J. Spacecr. Rockets*, vol. 39, no. 6, pp. 894–903, 2002.

[10] G. J. M. Hagelaar, J. Bareilles, L. Garrigues, and J.-P. Boeuf, "Two-dimensional model of a stationary plasma thruster," *J. Appl. Phys.*, vol. 91, no. 9, pp. 5592–5598, May 2002.

[11] M. Andrenucci, L. Biagioni, A. Passaro, "PIC/DSMC models for Hall effect thruster plumes: Present status and ways forward," presented at the 38th Joint Propulsion Conf., Indianapolis, IN, 2002, AIAA Paper 2002-4254.

[12] F. Taccogna, S. Longo, and M. Capitelli, "Very-near-field plume simulation of a stationary plasma thruster," *Eur. Phys. J., Appl. Phys.*, vol. 28, no. 1, pp. 113–122, 2004.

[13] F. Taccogna, S. Longo, and M. Capitelli, "Particle-in-cell with Monte Carlo simulation of SPT-100 exhaust plumes," *J. Spacecr. Rockets*, vol. 39, no. 3, pp. 409–419, 2002.

[14] L. Garrigues, J. Bareilles, J.-P. Boeuf, and I. D. Boyd, "Modeling of the plasma jet of a stationary plasma thruster," *J. Appl. Phys.*, vol. 91, no. 12, pp. 9521–9528, Jun. 2002.

[15] I. D. Boyd and R. A. Dressler, "Far field modeling of the plasma plume of a Hall thruster," *J. Appl. Phys.*, vol. 92, no. 4, pp. 1764–1774, Aug. 2002.

[16] A. Cohen-Zur, A. Fruchtman, and A. Gany, "Analysis of the Hall thruster plume divergence in the near and far fields," presented at the 28th Int. Electric Propulsion Conf., Toulouse, France, 2003, Paper IEPC 03-063.

[17] L. B. King and A. D. Gallimore, "Ion energy diagnostics in the plume of an SPT-100 from thrust axis to backflow region," *J. Propuls. Power*, vol. 20, no. 2, pp. 228–242, Mar./Apr. 2004.

[18] I. D. Boyd and J. T. Yim, "Modeling of the near field plume of a Hall thruster," *J. Appl. Phys.*, vol. 95, no. 9, pp. 4575–4584, May 2004.
[19] S. Cheng, M. Santi, M. Celik, M. Martinez-Sanchez, and J. Peraire, "Hybrid PIC-DSMC simulation of a Hall thruster plume on unstructured grids," *Comput. Phys. Commun.*, vol. 164, no. 1–3, pp. 73–79, Dec. 2004.
[20] A. Fruchtman and A. Cohen-Zur, "Plume divergence in the Hall thruster," presented at the 40th Joint Propulsion Conf. and Exhib., Fort Lauderdale, FL, Jul. 11–14, 2004, AIAA Paper No. 2004-3957.
[21] B. E. Beal, A. D. Gallimore, and W. A. Hargus, Jr., "Plasma properties downstream of a low-power Hall thruster," *Phys. Plasmas*, vol. 12, no. 12, p. 123 503, Dec. 2005.
[22] Y. Raitses, D. Staack, A. Smirnov, and N. J. Fisch, "Space charge saturated sheath regime and electron temperature saturation in Hall thrusters," *Phys. Plasmas*, vol. 12, no. 7, p. 073 507, Jul. 2005.
[23] V. Vial, S. Mazouffre, M. Prioul, D. Pagnon, and A. Bouchoule, "CCD images of Hall effect thruster plume dynamics after ultrafast current ignition," *IEEE Trans. Plasma Sci.*, vol. 33, no. 2, pp. 524–525, Apr. 2005.
[24] M. Keidar and I. D. Boyd, "On the magnetic mirror effect in Hall thrusters," *Appl. Phys. Lett.*, vol. 87, no. 12, p. 121 501, Sep. 2005.
[25] M. L. R. Walker, R. R. Hofer, and A. D. Gallimore, "Ion collection in Hall thruster plumes," *J. Propuls. Power*, vol. 22, no. 1, pp. 205–209, Jan./Feb. 2006.
[26] G. F. Karabadzhak, Y. H. Chiu, and R. A. Dressler, "Passive optical diagnostic of Xe propelled Hall thrusters—Part II: Collisional-radiative model," *J. Appl. Phys.*, vol. 99, no. 11, p. 113 305, Jun. 2006.
[27] A. Fruchtman and A. Cohen-Zur, "Plasma lens and plume divergence in the Hall thruster," *Appl. Phys. Lett.*, vol. 89, no. 11, p. 111 501, Sep. 2006.
[28] J. A. Linnell and A. D. Gallimore, "Internal plasma potential measurements of a Hall thruster using plasma lens focusing," *Phys. Plasmas*, vol. 13, no. 10, p. 103 504, Oct. 2006.
[29] I. D. Boyd, "Numerical simulation of Hall thruster plasma plumes in space," *IEEE Trans. Plasma Sci.*, vol. 34, no. 5, pp. 2140–2147, Oct. 2006.
[30] Y. Raitses, A. Smirnov, and N. J. Fisch, "Enhanced performance of cylindrical Hall thrusters," *Appl. Phys. Lett.*, vol. 90, no. 22, p. 221 502, May 2007.
[31] E. Ahedo, J. M. Gallardo, and M. Martinez-Sanchez, "Model of the plasma discharge in a Hall thruster with heat conduction," *Phys. Plasmas*, vol. 9, no. 9, pp. 4061–4070, Sep. 2002.
[32] E. Ahedo, P. Martinez-Cerezo, and M. Martinez-Sanchez, "One-dimensional model of the plasma flow in a Hall thruster," *Phys. Plasmas*, vol. 8, no. 6, pp. 3058–3068, Jun. 2001.
[33] A. Cohen-Zur, A. Fruchtman, J. Ashkenazy, and A. Gany, "Analysis of the steady-state axial flow in the Hall thruster," *Phys. Plasmas*, vol. 9, no. 10, pp. 4363–4374, Oct. 2002.

Avi Cohen-Zur was born in Tel Aviv, Israel, in 1968. He received the B.Sc., M.Sc., and Ph.D. degrees in aerospace engineering from the Technion—Israel Institute of Technology, Haifa, Israel, in 1994, 1998, and 2008, respectively. His M.Sc. thesis was an experimental study of the supersonic combustion of solid fuel scramjet engines. The presented work describes a part of his Ph.D. research on the theoretical study of the Hall thruster and its operating characteristics.

From 1994 to 2001, he was a Graduate Teaching Assistant with the Faculty of Aerospace Engineering, Technion—Israel Institute of Technology. During 2001–2002, he was a Research Assistant at H.I.T.—Holon Institute of Technology, Holon, Israel. Since 2002, he has been with WALES, Ltd., Ramat Gan, Israel, as an Aerospace Engineering Researcher. His main research interests include electrical and chemical propulsion, air breathing propulsion, combustion, plasma physics, thermodynamics and related areas, and aerospace system engineering.

Amnon Fruchtman (SM'08) was born in Rehovot, Israel. He received the B.Sc. degree from Tel Aviv University, Tel Aviv, Israel, in 1973, and the M.Sc. and Ph.D. degrees from the Hebrew University of Jerusalem, Jerusalem, Israel, in 1976 and 1983, respectively, all in physics.

After being a Postdoctoral Fellow with Courant Institute, he joined the Weizmann Institute of Science, Rehovot, which he left as an Associate Professor in 1995. He is currently a Professor with the Department of Sciences, H.I.T.—Holon Institute of Technology, Holon, Israel. He spent sabbaticals at Princeton University, Princeton, NJ, from 1994 to 1995, and with Ecole Polytechnique, France, in 2004. His areas of interest are free electron lasers, high-power pulsed plasmas, helicon and other plasma sources, and electric propulsion.

Prof. Fruchtman is a Fellow of the American Physical Society.

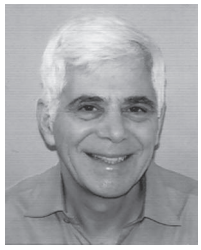

Alon Gany received the B.Sc. degree in chemical engineering, the M.Sc. degree, and the D.Sc. degree in aeronautical engineering from Technion—Israel Institute of Technology, Haifa, Israel, in 1968, 1971, and 1975, respectively.

He is currently a Professor holding the Lena and Ben Fohrman Chair in Aeronautical Engineering and heading the Sylvia and David I. A. Fine Rocket Propulsion Center at the Faculty of Aerospace Engineering and Asher Space Research Institute, Technion—Israel Institute of Technology. He was a Postdoctoral Fellow with Princeton University, Princeton, NJ, from 1976 to 1979. He spent a sabbatical year as a Senior Research Fellow with the U.S. Naval Postgraduate School, Monterey, CA, during 1983–1984, and another sabbatical year as a Visiting Professor with Princeton University during 1994–1995. He has supervised more than 70 masteral and doctoral students. He has authored over 80 published refereed journal articles and some 240 presentations in professional conferences. His main research interests are propulsion, combustion, energy, and related areas.

Prof. Gany is a member of the International Academy of Astronautics, an Honorary Fellow of the High Energy Materials Society of India, a Fellow of the American Institute of Aeronautics and Astronautics, a Fellow of the Royal Institution of Naval Architects, and a member of the American Society of Mechanical Engineers, the Combustion Institute, and the Israel Society of Aeronautics and Astronautics.